

An Advanced Current Control Strategy for Three-Phase Shunt Active Power Filters

Quoc-Nam Trinh and Hong-Hee Lee, *Senior Member, IEEE*

Abstract—This paper proposes an advanced control strategy to enhance performance of shunt active power filter (APF). The proposed control scheme requires only two current sensors at the supply side and does not need a harmonic detector. In order to make the supply currents sinusoidal, an effective harmonic compensation method is developed with the aid of a conventional proportional-integral (PI) and vector PI controllers. The absence of the harmonic detector not only simplifies the control scheme but also significantly improves the accuracy of the APF, since the control performance is no longer affected by the performance of the harmonic tracking process. Furthermore, the total cost to implement the proposed APF becomes lower, owing to the minimized current sensors and the use of a four-switch three-phase inverter. Despite the simplified hardware, the performance of the APF is improved significantly compared to the traditional control scheme, thanks to the effectiveness of the proposed compensation scheme. The proposed control scheme is theoretically analyzed, and a 1.5-kVA APF is built in the laboratory to validate the feasibility of the proposed control strategy.

Index Terms—Active power filters (APFs), harmonic current compensation, power quality, resonant controller.

I. INTRODUCTION

THE INCREASING use of nonlinear loads such as adjustable speed drives, electric arc welders, and switching power supplies causes large amounts of harmonic currents inject into distribution systems. These harmonic currents are responsible for voltage distortion, increasing power losses and heat on networks and transformers, and causing operational failure of electronic equipment. Due to these problems, harmonic restriction standards such as IEEE-519 or IEC 61000-3-2 have been published to demand those harmonic currents injected into utility networks to be below the specified values [1], [2]. In order to improve the power quality of distribution networks as well as to meet these restriction standards, two main solutions have been introduced: LC passive filters and active power filters (APFs) [3]–[5].

LC passive filters are traditionally utilized to compensate the harmonic currents since they are simple and low-cost solution. However, they are often large and heavy. Furthermore, the compensation capability of a passive filter is typically fixed

Manuscript received May 1, 2012; revised August 20, 2012; accepted October 16, 2012. Date of publication December 10, 2012; date of current version June 21, 2013. This work was supported by the 2013 Research Fund of the University of Ulsan.

The authors are with the School of Electrical Engineering, University of Ulsan, Ulsan 680-749, Korea (e-mail: hhlee@mail.ulsan.ac.kr; trinhquocnam2010@gmail.com).

Color versions of one or more of the figures in this paper are available online at <http://ieeexplore.ieee.org>.

Digital Object Identifier 10.1109/TIE.2012.2229677

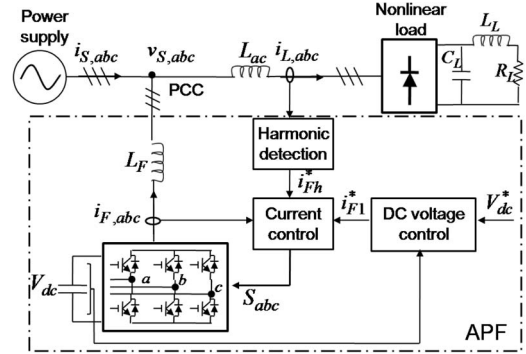


Fig. 1. Typical control scheme of a shunt APF.

and relies heavily on a network's impedance, thus potentially causing undesired resonance problems [5].

In contrast, shunt APFs are recognized as a flexible solution for harmonic current compensation since they are capable of compensating harmonic currents generated by many types of nonlinear loads as well as providing fast responses to load variations [3]–[5]. A typical control scheme of a shunt APF is illustrated in Fig. 1. The purpose of an APF is to generate harmonic currents ($i_{F,abc}$) having the same magnitude and opposite phase with the harmonics produced by the nonlinear load, and to ensure that the supply currents ($i_{S,abc}$) contain only the fundamental component. In order to realize the desired goals, as shown in Fig. 1, the traditional control scheme requires several steps such as load current measurement, harmonic current detection, reference filter current generation, and filter current control [6]–[13], [15]–[18]. Since the APF must generate non-sinusoidal currents, the design of the current controller for the APF is a challenging task. Various control methods have been developed in the literature such as proportional-integral (PI) control [6], [8]–[10], dead-beat control [7], and hysteresis control [6]. Due to the limitation of the control bandwidth, the PI controller is not a suitable solution for the APF applications since the current controller must deal with harmonic currents, which are high-frequency signals. In contrast, the dead-beat control method is able to provide fast control response, but the control performance relies significantly on knowledge of the APF parameters. Despite the simple and robust feature of the hysteresis controller, this approach also has an inherent drawback: switching frequency variation, which causes a difficulty in design of an output filter for the APF and results in unwanted resonance problems with the networks. In addition, in order to achieve good current performance, the hysteresis band must be set as small as possible. It results in a significant

increasing of the switching frequency and consequently introduces higher switching loss on the APF.

In recent years, several high-performance current controllers have been developed for APFs to achieve good control performance [15]–[18]. In these control schemes, the current controllers are employed in the fundamental reference frame, consisting of a proportional controller plus multiple sinusoidal signal integrators [15], a PI controller plus a series of resonant controllers [16], [17], or vector PI (VPI) controllers [18]. In fact, the VPI controller introduced in [18] is an alternative version of resonant controller that has superior and robust characteristics when compensating high-order harmonic currents. These control schemes are capable of providing good control performances thanks to high-performance current controllers. However, as illustrated in Fig. 1, the performance of the APF relies on not only the current controller but also the harmonic currents detector. The harmonic detector aims to extract the harmonic components presented in the load currents whose output becomes the reference filter current for the APF. Thus, the performance of this process critically impacts on the accuracy of the APF. The harmonic detector is typically employed by using filters such as high-pass, low-pass, adaptive filters [8]–[13], or through complex mathematical functions [14]. However, by using these filters, it is difficult to achieve both fast response and good steady-state harmonic tracking performance because of a compromise: if the filters are designed to achieve good steady-state performance, their response becomes slow and vice-versa. As a result, the use of a harmonic detector in the control scheme may have an adverse effect on both the accuracy and response of an APF.

In order to avoid the use of harmonic detectors, indirect current control schemes have been introduced in [19]–[24] where the supply currents ($i_{S,abc}$) are directly measured and regulated to be sinusoidal. In [19], [20], [22], hysteresis controller was used in the current control loop to force the supply current to be sinusoidal. However, as mentioned earlier, this method has a drawback, i.e., the variation of the switching frequency, so that the supply current regularly contains many switching noises. Meanwhile, the PI controller and the proportional controller are utilized in [21] and [23], respectively. They obviously have a limitation on the control bandwidth and are unable to accurately regulate high-frequency signals such as harmonic currents. Consequently, it is hard to achieve a good performance of the supply currents. In [24], authors demonstrated that indirect control method is able to provide better performances compared to direct one since it can prevent inaccurate tracking performances of the harmonic detector. Nevertheless, in this control scheme, two sets of current sensors are required. In addition, the reference supply current is given based on the supply voltage which is assumed to be a pure sinusoidal waveform. Thus, the performance of the supply current is degraded when the supply voltage is distorted.

Adopting the advantage of indirect current control schemes, i.e., the absence of a harmonic detector, this paper proposes an advanced control strategy to enhance the APF performance. In the proposed control scheme, the supply currents are directly measured and regulated to be sinusoidal by an effective harmonic compensator, which is developed based on a PI plus

VPI controllers and implemented in the fundamental reference frame. Owing to the effectiveness of the proposed PI-VPI controller, the harmonic currents produced by the nonlinear load can be accurately compensated without the demand of a load current measurement and harmonic detector. The absence of the harmonic detector not only simplifies the control scheme but also significantly improves the accuracy of the APF since the control performance is no longer affected by the performance of the harmonic tracking process. Moreover, the total cost to implement the proposed APF is lower, owing to the minimized current sensors and the use of a four-switch three-phase inverter (FSTPI). Despite the simplified hardware, the performance of the APF is significantly improved compared to the traditional control scheme thanks to the superiority of the proposed compensation scheme. And also, the proposed control algorithm is capable of mitigating harmonic currents as well as reactive power to achieve unity power factor condition at the supply side. The proposed control scheme is theoretically analyzed, and a 1.5-kVA APF is built in the laboratory to validate the feasibility of the proposed control strategy.

II. PROPOSED CONTROL STRATEGY TO IMPROVE APF PERFORMANCE

A. Structure of a Shunt APF

Three-phase diode rectifiers are widely used as the front-ends of industrial ac drives [3]–[5]. These types of loads introduce harmonic currents into the networks, which have odd orders: $6n \pm 1$ ($n = 1, 2, 3, \dots$) of the fundamental frequency. Since these harmonic currents cause serious problems and deteriorate the power quality of the distribution networks, the shunt APF was developed to compensate those harmonic currents and consequently to improve the power quality.

As illustrated in Fig. 1, a shunt APF is basically a three-phase voltage source inverter (VSI) connected in parallel with a nonlinear load at the point of common coupling through an inductor L_F . The energy storage of the APF is a large capacitor located at the dc-link side of the inverter. The nonlinear load can be presented as a RL or RLC load connected to the power supply through a three-phase diode rectifier as shown in Fig. 1. As stated earlier, the APF must generate the harmonic currents to compensate harmonics produced by the nonlinear load and to make the supply currents sinusoidal. To fulfill these demands, the traditional control scheme requires a harmonic detector and current controller where both loops must be designed properly to achieve good control performance. However, it may cause excessive complexity in the design process.

B. Proposed Control Strategy

In order to simplify the control scheme and to enhance the accuracy of the APF, an advanced control strategy is proposed, as shown in Fig. 2. In Fig. 2, the proposed control scheme is implemented by using only the supply current (i_{S_a} and i_{S_b}) without detecting the load current ($i_{L,abc}$) and filter current ($i_{F,abc}$). Thereby, the load current sensors and filter current sensors in the typical shunt APF shown in Fig. 1 can be

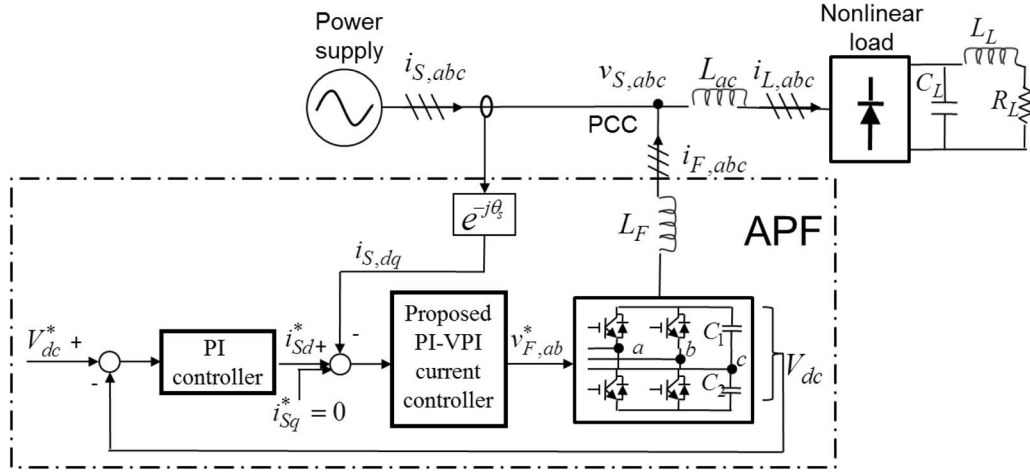


Fig. 2. Structure of the proposed control scheme for three-phase shunt APF.

eliminated. And also, the harmonic current detection is omitted. Due to the absence of harmonic detection, the proposed control scheme can be implemented with only two loops: the outer voltage control and the inner current control. The outer loop aims to keep dc-link voltage of the APF constant through a PI controller, which helps the APF deal with load variations. The output of this control loop is the reference active current in the fundamental reference frame (i_{Sd}^*). Meanwhile, the reference reactive current (i_{Sq}^*) is simply set to be zero, which ensures the reactive power provided by the power supply to be zero. And, the reactive power caused by loads is supplied by the shunt APF. The inner loop is then used to regulate the supply current in the fundamental reference frame ($i_{S,dq}$) by using the proposed PI-VPI current controller. The output of this loop becomes the control signal ($v_{F,ab}^*$) applied to the four-switch APF which is implemented by the FSTPI. Since the current control is executed without the harmonic detector, the control performance of the APF only relies on the current controller. In the next section, the analysis and design of the proposed current controller will be presented.

III. CURRENT CONTROL SCHEME USING PI PLUS VPI CONTROLLERS IN FUNDAMENTAL REFERENCE FRAME

A. Proposed Current Controller

As illustrated in Fig. 1, harmonic components are detected from the load current by means of the harmonic detector whose output is the reference filter current for the APF. Since the reference filter current is a non-sinusoidal signal, design of current controller for an APF is a challenging task. A series of resonant controllers tuned at harmonic frequencies is typically required for achieving good current performance [15]–[18].

In contrast, in the proposed control scheme shown in Fig. 2, the supply current is directly sensed, and the current controller is executed to regulate the supply current to be sinusoidal. Normally, a conventional PI controller employed in the fundamental reference frame is sufficient for regulating the sinusoidal signals since these signals behave as dc signals in this frame. However, in the APF system, it is impossible to force the supply currents to be sinusoidal by using only a PI controller because

the supply currents are not directly but indirectly controlled by regulating the filter currents which are the non-sinusoidal signals. In fact, due to the limitation of the control bandwidth, the PI controller is unable to adequately regulate the high-frequency signals, e.g., harmonic currents. As a result, the desired control target of the APF cannot be achieved by using only PI current controller in [21].

In order to effectively regulate the supply currents to be sinusoidal, the current controller must have high gains at harmonic frequencies, which can be achieved by means of multiple resonant controllers tuned at harmonic frequencies. The transfer function of multiple proportional resonant controllers in the s-domain is given as

$$G_{PR} = \sum_{h=1,5,7,11,13,\dots} K_{ph} + \frac{2K_{rh}s}{s^2 + (h\omega_s)^2} \quad (1)$$

where K_{ph} and K_{rh} are the proportional and resonant gains of the resonant controller, respectively, h is the order of harmonic currents, and ω_s is the fundamental frequency of the supply voltage.

However, as shown in (1), each resonant controller has a responsibility to regulate only one harmonic component. Thus, the controller complexity and computational burden are significantly increased if large numbers of harmonic currents are required to be compensated.

In fact, each pair of $h = 6n \pm 1$ harmonic currents behave as $h = 6n$ harmonic currents in the fundamental reference frame. Thus, it is possible to perform a resonant controller tuned at $h = 6n$ multiples of ω_s in this reference frame to regulate a pair of $h = 6n \pm 1$ harmonic currents. The transfer function of the PI controller plus resonant controllers in the s-domain is given as

$$G_{PI-R} = K_{p1} + \frac{K_{i1}}{s} + \sum_{h=6,12,18,\dots} K_{ph} + \frac{2K_{rh}s}{s^2 + (h\omega_s)^2} \quad (2)$$

where K_{p1} and K_{i1} are the proportional and integrator gains of the PI controller, respectively, $h = 6n$ is the order of harmonics in the fundamental reference frame with $n = 1, 2, 3, \dots$

In (2), the aim of the PI controller is to regulate the fundamental current whereas resonant controllers are used to control

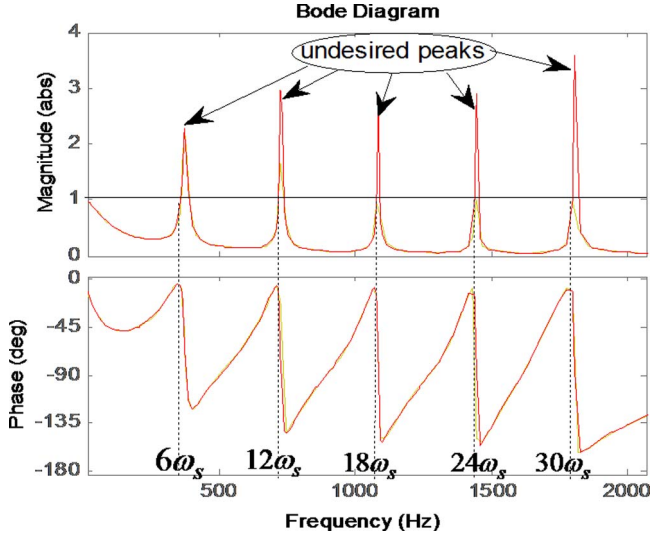


Fig. 3. Closed-loop Bode diagram of PI-R controller with compensation method given in (3) with $N = 2$, $h = 6n$, and $n = 1 \dots 5$.

the harmonic currents. However, the delay time caused by the effect of the APF and digital implementation must be taken into account if the high-order harmonics are compensated [17], [25], [26]. A compensation term is added to (2) to compensate the delay time, the transfer function of the PI-R controller becomes

$$G_{\text{PI-R}} = K_{p1} + \frac{K_{i1}}{s} + \sum_{h=6,12,18,\dots} K_{ph} + 2K_{rh} \frac{s \cos(h\omega_s NT_s) - h\omega_s \sin(h\omega_s NT_s)}{s^2 + (h\omega_s)^2} \quad (3)$$

where N is the number of samples and T_s is the sampling period. As described in [17], the best result is obtained when $N = 2$.

The compensation method given in (3) only considers the delay time caused by digital implementation and neglect the effect of the APF: the stability margins are reduced, and undesired peaks appear in the closed-loop frequency response when the order of the compensated harmonic increases as shown in Fig. 3. In order to overcome these problems, an alternative solution of the resonant controller, the VPI controller, has been introduced [18]. The transfer function of the VPI controllers in the s-domain is

$$G_{\text{VPI}} = \sum_{h=6,12,18,\dots} 2 \frac{K_{ph}s^2 + K_{rh}s}{s^2 + (h\omega_s)^2}. \quad (4)$$

The VPI controller is able to cancel the coupling term with the form $1/(sL_F + R_F)$ by selecting the resonant gain as $K_{rh} = K_{ph}R_F/L_F$, where L_F and R_F are the inductance and the equivalent resistance of the L_F inductor, respectively. Owing to this advantage, the VPI controller is able to remove anomalous peaks appearing in the closed-loop response without demand of delay compensation. Adopting the superiority of the VPI controllers over resonant controllers, VPI controllers given in (4) are used to replace resonant controllers in (2), the

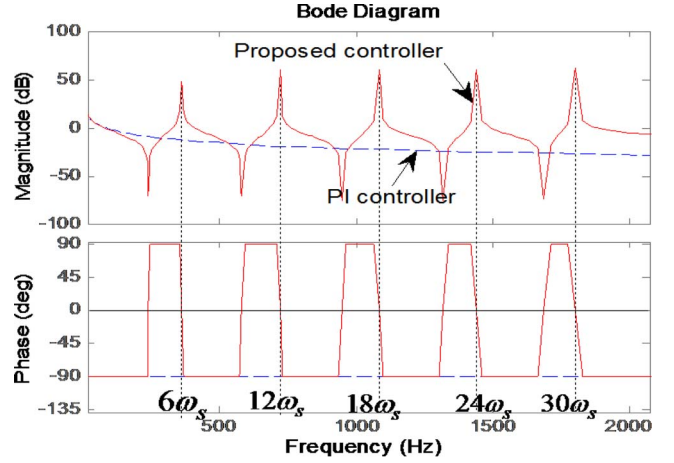


Fig. 4. Open-loop Bode diagrams of the conventional PI and proposed controller.

transfer function of the proposed PI-VPI current controller in the s-domain is given as follows:

$$G_{\text{PI-VPI}} = K_{p1} + \frac{K_{i1}}{s} + \sum_{h=6,\dots,30} 2 \frac{K_{ph}s^2 + K_{rh}s}{s^2 + (h\omega_s)^2}. \quad (5)$$

In order to investigate the superior characteristics of the proposed PI-VPI controller over the traditional PI controller, Fig. 4 describes open-loop Bode diagram for the traditional PI and the proposed controllers given in (5) for the case of $h = 6n$, $n = 1 \dots 5$, $\omega_s = 2\pi 60$ rad/s, $K_{ph} = 1$, and $K_{rh} = K_{ph}R_F/L_F$. As illustrated in Fig. 4, at low frequency (less than 20 Hz), the gains of both the PI and proposed controllers are high and comparable, but at high frequencies, i.e., selected resonant frequencies ($6\omega_s$, $12\omega_s$, $18\omega_s$, $24\omega_s$, and $30\omega_s$), the gain of the PI controller is significantly reduced while the proposed controller produces very high gains for ensuring zero steady-state errors in compensating the harmonic currents.

As mentioned earlier, the PI-R controller given in (3) is also able to produce high gains at selected resonant frequencies and overcome the limitation of the PI controller. However, as presented in Fig. 3, undesired peaks appear in the closed-loop frequency response of the PI-R controller when it compensates high-order harmonic components. In contrast, the proposed PI-VPI controller is capable of preventing this problem owing to its pole-zero cancellation capability with the L_F inductor.

Taking into account the L_F inductor model defined by (6), the closed-loop transfer function of the proposed current control is defined in (7), shown at the bottom of the next page

$$G_{L_F} = \frac{1}{sL_F + R_F}. \quad (6)$$

Fig. 5 presents the Bode diagram of the closed-loop transfer function for the proposed controller and the PI-R controller with $h = 6n$, $n = 1 \dots 5$, $K_{ph} = 1$, and $K_{rh} = K_{ph}R_F/L_F$. As shown in Fig. 5, the proposed controller provides unity gain and zero phase-shift for all selected resonant frequencies while there are undesired peaks in the closed loop of the PI-R

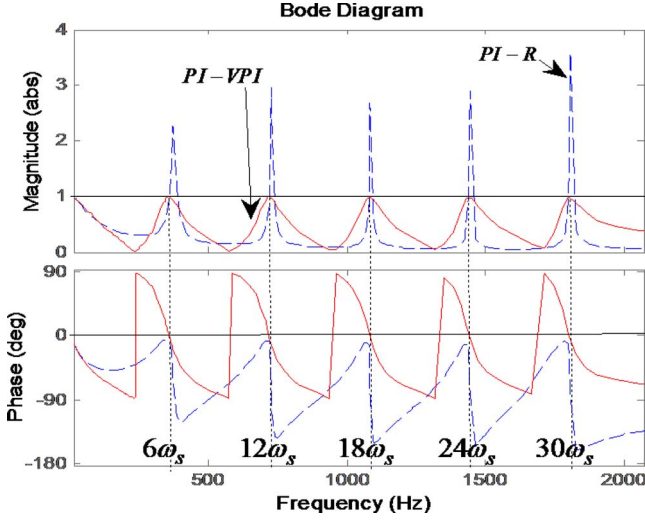


Fig. 5. Closed-loop Bode diagrams of the PI-VPI and PI-R controller.

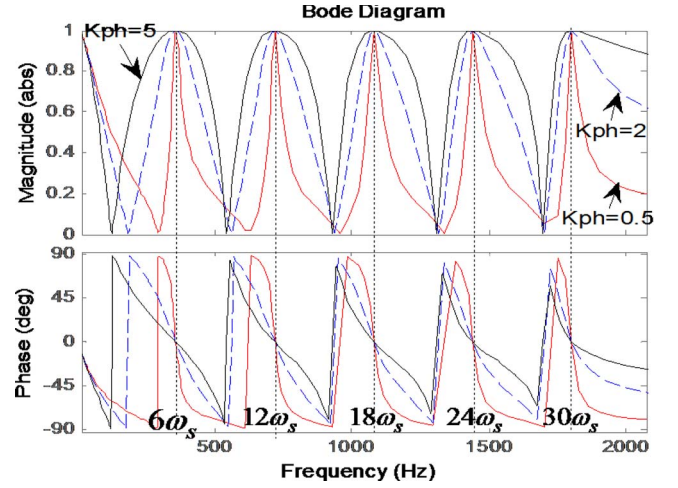


Fig. 7. Closed-loop Bode diagrams of the VPI controllers with $K_{ph} = 0.5$, $K_{ph} = 2$, and $K_{ph} = 5$.

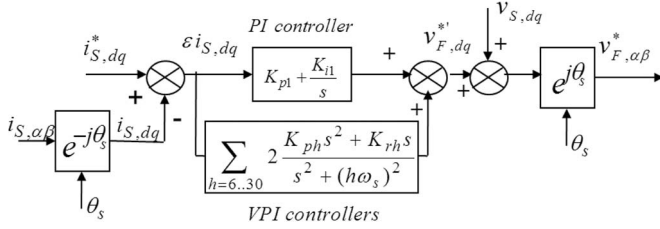


Fig. 6. Block diagram of the proposed current control scheme.

controller. Thus, the use of VPI controllers significantly improves the stability margin and accuracy of the proposed current controller.

The complete proposed current control scheme using the PI-VPI controller is shown in Fig. 6. Since the proposed current controller is designed in the fundamental reference frame, the measured supply current $i_{S,\alpha\beta}$ first must be transformed from the stationary to the fundamental reference frame $i_{S,dq}$. The proposed current controller is then executed to regulate this current follow its reference $i_{S,dq}^*$. The outputs of the current controllers $v_{F,dq}^*$ and the feedforward supply voltage term $v_{S,dq}$ are added together and then transformed in the stationary reference frame through an inverse rotational transformation to obtain the command voltage $v_{F,\alpha\beta}^*$, which is the control signal for the APF.

B. Current Controller Design

In order to design the gains for the PI-VPI controller and to investigate the effect of these gains on the control performance, the closed-loop transfer function of the PI-VPI current controller defined in (7) is analyzed. By selecting the resonant gain as $K_{rh} = K_{ph}R_F/L_F$ and $K_{i1} = K_{p1}R_F/L_F$, the closed-loop transfer function of the PI-VPI controller becomes (8), shown at the bottom of the page.

In (8), K_{ph} and K_{p1} are the only gains that need to be tuned. In fact, K_{p1} is the integrator gain of the PI controller that does not affect the harmonic compensation performance of the VPI controller. Thus, for the sake of simplification, K_{p1} is kept constant, and K_{ph} is changed to determine the control performance of the VPI controller. The Bode diagram is illustrated in Fig. 7 with $K_{ph} = 0.5$, $K_{ph} = 2$, and $K_{ph} = 5$. As shown in Fig. 7, at selected resonant frequencies, the VPI controller provides a unity gain and zero phase-shift, regardless of the value of K_{ph} . Moreover, the narrowest bandwidth is achieved with $K_{ph} = 0.5$, which indicates that the VPI controller is more selective and obtain better steady-state performance if K_{ph} is a smaller value. In harmonic compensation application, the steady-state performance is regarded as the most critical index; thus it prefers to choose K_{ph} to be a small value ($K_{ph} < 1$).

$$G_C = \frac{G_{PI-VPI}G_{L_F}}{1 + G_{PI-VPI}G_{L_F}} = \sum_{h=6\dots30} \frac{(K_{p1} + 2K_{ph})s^3 + (K_{i1} + 2K_{rh})s^2 + K_{p1}(h\omega_s)^2s + K_{i1}(h\omega_s)^2}{L_F s^4 + (K_{p1} + 2K_{ph} + R_F)s^3 + (K_{i1} + 2K_{rh} + L_F(h\omega_s)^2)s^2 + (R_F + K_{p1})(h\omega_s)^2s + K_{i1}(h\omega_s)^2} \quad (7)$$

$$G_C = \sum_{h=6\dots30} \frac{(K_{p1}L_F + 2K_{ph})s^2 + 2K_{ph}K_{p1}s + K_{p1}L_F(h\omega_s)^2}{L_F s^3 + (K_{p1}L_F + 4K_{ph})s^2 + (2K_{ph}K_{p1} + L_F(h\omega_s)^2)s + K_{p1}L_F(h\omega_s)^2} \quad (8)$$

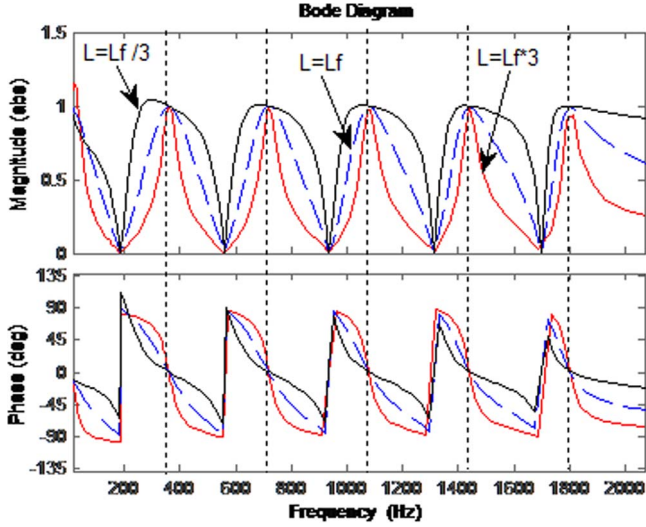


Fig. 8. Closed-loop Bode diagrams of the VPI controllers with variation of the inductor parameters.

However, we should not select a too small K_{ph} since it may degrade the dynamic responses of the APF.

The controller gains obtained by using aforementioned design process are kept constant during whole operating time. However, the inductor parameters are changed during operation, so that the relationship, $K_{rh} = K_{ph}R_F/L_F$, is no longer satisfied. Fig. 8 shows the Bode diagram of (7) in order to investigate the robustness of the VPI controller against the inductor parameter variation. As can be seen in Fig. 8, the VPI controller still maintains a unity gain and zero phase-shift at a selected resonant frequency regardless of the different inductor parameter, which means that the inductor parameter variation has no effect on the stability and steady-state performance of the APF.

C. Discrete-Time Implementation of the VPI Controllers

An important step to realize any digital controller is discretization, which transfers the controller from the continuous-time to the discrete-time type to be implemented with digital processors such as microcontrollers or digital signal processors (DSPs). Because of the narrow band and infinite gain characteristics of the resonant and VPI controllers, a slight displacement of the resonant poles causes a significant loss of performance. Therefore, the selection of a discretization technique is critical and significantly impacts on the accuracy and control performance of the VPI controllers [25]. As analyzed in [26], to achieve accurate resonant pole placement, the transfer function of the VPI controller in the z -domain must be determined as follows:

$$G_{VPI}(z) = \frac{K_{ph} + (K_{rh}T_s - 2K_{ph})z^{-1} - (K_{rh}T_s - K_{ph})z^{-2}}{1 - 2\cos(h\omega_s T_s)z^{-1} + z^{-2}} \quad (9)$$

where z is the shift operator.

The transfer function given in (9) provides an accurate resonant pole placement, but the trigonometric portion of the formula, i.e., the cosine function, must be online calculated and consumes a large amount of execution time as part of the control scheme, particularly when the control algorithm is

implemented in low-performance microprocessors or DSPs. So as to avoid this large calculation time, the cosine function is approximated by means of a Taylor series as given by

$$\cos(h\omega_s T_s) = 1 - \frac{(h\omega_s T_s)^2}{2} + \frac{(h\omega_s T_s)^4}{24} - \frac{(h\omega_s T_s)^6}{720} + \dots \quad (10)$$

A higher order approximation results in a more precise result, but an approximation of fourth order also can provide sufficient accuracy and high performance with significantly reduced computation time for the VPI controllers [26]. Therefore, a fourth-order approximation is used to replace the cosine function in (9). The transfer function of the VPI controller in the z -domain can now be rewritten as

$$G_{VPI}(z) = \frac{K_{ph} + (K_{rh}T_s - 2K_{ph})z^{-1} - (K_{rh}T_s - K_{ph})z^{-2}}{1 - 2\left(1 - \frac{(h\omega_s T_s)^2}{2} + \frac{(h\omega_s T_s)^4}{24}\right)z^{-1} + z^{-2}} \quad (11)$$

IV. DESCRIPTION OF THE WHOLE CONTROL STRATEGY

Fig. 9 illustrates the block diagram of whole proposed control strategy. As aforementioned, the proposed control scheme contains two main loops: the dc-link voltage control and the supply current control. In addition, since the proposed current controller is employed in the fundamental reference frame, a phase-locked loop (PLL) is required to track the phase of the supply voltage which is needed for coordinate transformation and synchronization.

A. DC-Link Voltage Control Loop

As stated earlier, this control loop aims to keep dc-link voltage of the shunt APF constant through a simple PI regulator, whose output is the reference active current in the fundamental reference frame as follows:

$$i_{Sd}^* = \left(K_{pdc} + \frac{K_{idc}}{s}\right)(V_{dc}^* - V_{dc}) \quad (12)$$

where K_{pdc} and K_{idc} are the proportional and integrator gains of the PI controller, respectively, and V_{dc}^* and V_{dc} are reference and measured dc-link voltages of the APF, respectively.

In fact, since the four-switch APF has only two switching legs, the four-switch APF needs a higher dc-link voltage reference (V_{dc}^*) compared to the traditional six-switch APF as mentioned in Table I. In addition, since the dc-link voltage of the APF contains small ripples at harmonic frequencies due to harmonic currents, a low-pass filter (LPF) is designed to eliminate all ripples in the feedback measurement of the dc-link voltage, which helps in smoothing the reference current i_{Sd}^* .

In the proposed control scheme, the role of the dc-link voltage controller is not only to ensure a proper operation of the APF but also to help the APF deal with load variations. In this paper, even though the load current measurement is not used, the load changes can be detected indirectly through dc-link voltage variations. Hence, by detecting and regulating the

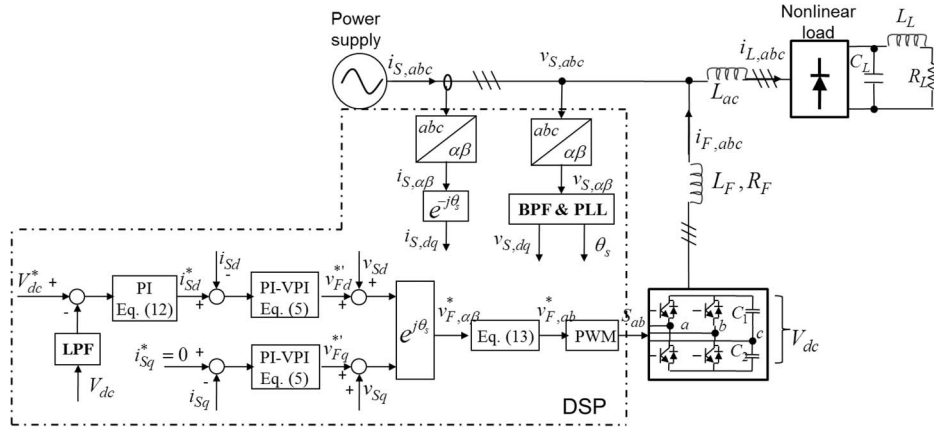


Fig. 9. Block diagram of the proposed control scheme.

TABLE I
SYSTEM PARAMETERS

Supply voltage RMS line-line	127 V
Supply frequency	60 Hz
5 th harmonic supply voltage	10% of the fundamental component
7 th harmonic supply voltage	5% of the fundamental component
DC-link reference voltage for the six-switch APF V_{dc}^*	260 V
DC-link reference voltage for the four-switch APF V_{dc}^*	420 V
DC-link capacitor for four-switch APF $C_1=C_2$	1000 μF
DC-link capacitor for six-switch APF $C=C_1+C_2$	2000 μF
Filter resistance R_F	0.05 Ω
Filter inductance L_F	2 mH
Nonlinear RLC load	$R_{L(\min)}=12.5 \Omega$, $R_{L(\max)}=20 \Omega$, $L_L=1 \text{ mH}$, $C_L=2200 \mu F$

dc-link voltage, the shunt APF can recognize and respond against load variations without the load current measurement.

B. Supply Current Control Loop

This loop regulates the supply current by means of the proposed current control scheme shown in Fig. 6. The reference active current i_{sd}^* is the output of the dc-link voltage control loop given in (13), while the reference reactive current i_{sq}^* is simply set to be zero. Consequently, the reactive power caused by loads can be fully compensated by the APF, and also unity power factor condition is achieved at the supply side.

C. Control Signal Computation for the Four-Switch APF

The traditional three-phase VSI is commonly used to implement an APF. In this paper, in order to accomplish a low-cost APF topology, the four-switch APF is introduced by replacing the traditional three-phase VSI with the FSTPI with-

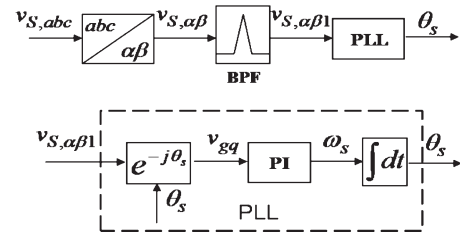


Fig. 10. Block diagram of the improved PLL.

out degrading the performance of the proposed control strategy. The FSTPI, which is composed of four power switching devices and two split capacitors, has been applied for low-cost ac motor drives [27], [28]. In Fig. 9, the control signal in the stationary reference frame ($v_{F,\alpha\beta}^*$) obtained after executing the current controller is changed into control signals of the four-switch APF as the following equations:

$$\begin{aligned} v_{Fa}^* &= \sqrt{\frac{3}{2}}v_{F\alpha}^* + \sqrt{\frac{1}{2}}v_{F\beta}^* \\ v_{Fb}^* &= \sqrt{2}v_{F\beta}^* \end{aligned} \quad (13)$$

where v_{Fa}^* and v_{Fb}^* are the control signals for leg a and b of the four-switch APF, respectively.

D. Supply Voltage PLL

The aim of this loop is to track the phase of the supply voltage, which is a necessary component for any converter interfacing with grid. In practical distribution network, supply voltage is regularly not pure sinusoidal but contains harmonic components, which may affect to the accuracy of the PLL. To overcome this problem, a bandpass filter (BPF) tuned at the fundamental frequency of the supply voltage is implemented to reject all of the harmonic components contained in supply voltage, and its output contains only the fundamental component which is used as the input of the PLL block. The block diagram of the improved PLL is illustrated in Fig. 10. Even though the BPF used in the PLL can cause a small time delay in tracking the phase angle of the supply voltage, it is negligible because the PLL usually operates at steady-state condition before the APF is active.

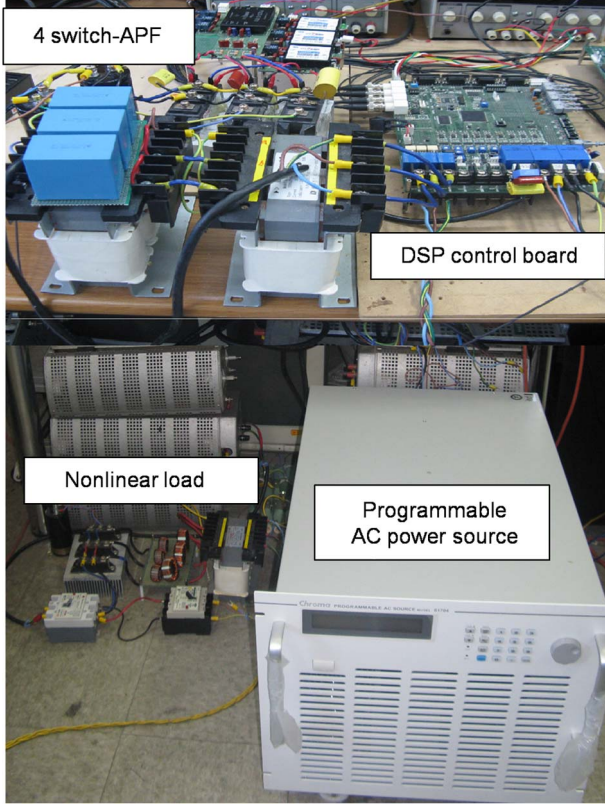


Fig. 11. Experiment platform of the four-switch three-phase shunt APF.

 TABLE II
 CURRENT CONTROLLER GAINS

$K_{p1} = 4$	$K_{i1} = 100$	$K_{p18} = 0.3$	$K_{r18} = 7.5$
$K_{p6} = 0.8$	$K_{r6} = 20$	$K_{p24} = 0.1$	$K_{r24} = 2.5$
$K_{p12} = 0.6$	$K_{r12} = 15$	$K_{p30} = 0.1$	$K_{r30} = 2.5$

V. EXPERIMENTAL RESULTS

An overview of the experimental system built in the laboratory is shown in Fig. 11. The system consists of a 1.5-kVA shunt APF and a 3-kVA nonlinear load with the parameters listed in Table I. The control algorithm was implemented using a 32-bit fixed point DSP (TMS320F2812 by Texas Instruments), with a 150-MHz clock frequency. The control sampling and switching frequencies are set at 10 kHz. The current controller is designed with one PI controller and five VPI controllers, capable of compensating all of the harmonic currents up to the 31st harmonic (1860 Hz). The gains of the controllers were individually tuned, as listed in Table II. The supply voltage is generated by a 6-kVA Programmable AC Power Source (Chroma 61704) that is able to produce either ideal sinusoidal or distorted supply voltage sources to investigate the performance of the proposed control strategy. Two types of nonlinear loads were used in the experimental tests, i.e., the RL and RLC loads connected to the power supply through a diode rectifier as shown in Fig. 9.

First, before evaluating the performance of the proposed APF, we have investigated the existing APF with the PI current controller by using the current control scheme in [21] because it uses the indirect current control method and its control scheme is similar to the proposed control strategy except the PI current

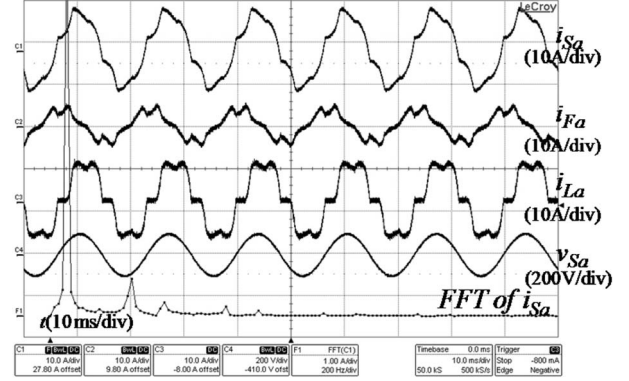


Fig. 12. Steady-state performance with PI current controller under RL load.

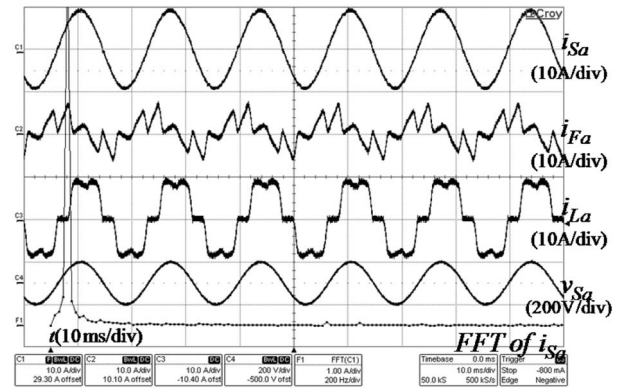
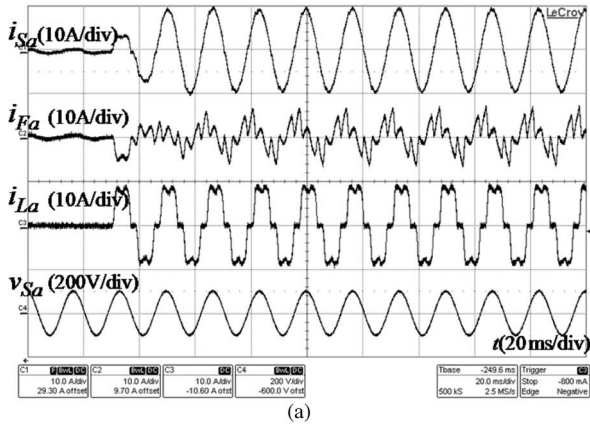


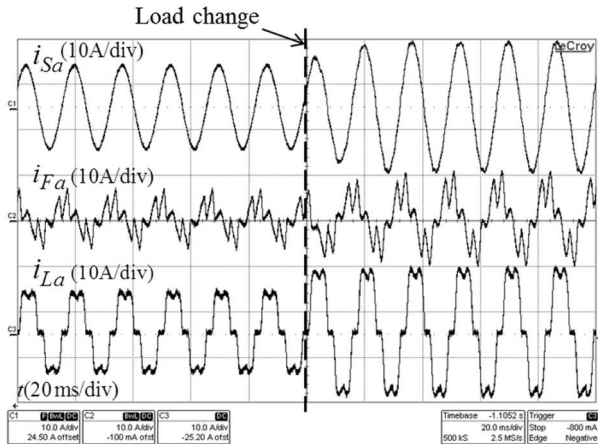
Fig. 13. Steady-state performance with proposed control scheme under RL load.

controller to regulate harmonic currents. The experiment is implemented with the nonlinear RL load, and the result is shown in Fig. 12, where the supply current i_{Sa} along with its fast Fourier transformation analysis, the filter current i_{Fa} of the APF, the load current i_{La} , and the supply voltage v_{Sa} are plotted. Fig. 12 shows that the harmonic currents are insufficiently compensated and the supply current is non-sinusoidal waveform with a high total harmonic distortion (THD) factor of approximately 11.3%. As described in Section III. A and shown in Fig. 4, the PI controller is unable to effectively compensate the harmonic currents due to its control bandwidth limitation. Hence, the desired control target of the APF cannot be achieved by using the traditional PI controller.

To demonstrate the superiority of the proposed control algorithm as compared to the traditional PI control scheme, an experimental test under the same condition as that shown in Fig. 12 was carried out by using the proposed control scheme. The results are presented in Fig. 13. Fig. 13 shows that the harmonic currents are effectively compensated and the supply current is almost sinusoidal with a small THD factor of approximately 1.65% whereas the load current is highly distorted with the THD factor of 25.2%. From these results, the effectiveness of the proposed control scheme is verified: harmonic currents are effectively compensated without load current measurement and harmonic detector. In addition, the proposed control scheme avoids the presence of notches in the supply current caused by the inaccurate harmonic tracking performance of the harmonic detector as reported in [13], [24].



(a)



(b)

Fig. 14. Dynamic responses of proposed control scheme under RL load variations: (a) load applied (b) load changed.

To evaluate the dynamic performance of the proposed control strategy with load variations, the transient responses of the APF with the load applied or changed are shown in Fig. 14(a) and (b), respectively. As shown in Fig. 14, as soon as the load is applied or changed, the filter current quickly responds to changes to compensate harmonic currents in the load and to ensure that the supply current sinusoidal and in-phase with the corresponding supply voltage. In fact, due to the effect of the LPF in the dc-link control loop, the response time of the supply current is minimally increased, but it is not longer than one period of the supply voltage.

Likewise, the proposed control strategy is also performed with a nonlinear RLC load, where the steady-state performance and dynamic response are shown in Figs. 15 and 16, respectively. In Fig. 15, the supply current is very close to sinusoidal with a low THD factor of approximately 1.72% while the THD of load current is very high, about 30.2%. In Fig. 16, the filter current also quickly responds to the load variations to compensate the harmonic currents in the supply. The supply current becomes close to sinusoidal with its response time of less than one period of the supply voltage.

It is verified through experiments that the proposed control strategy has good steady-state performances as well as good dynamic responses with both nonlinear RL and RLC loads.

In majority of previous studies, the supply voltage has usually been assumed to be an ideal sinusoidal, but this voltage

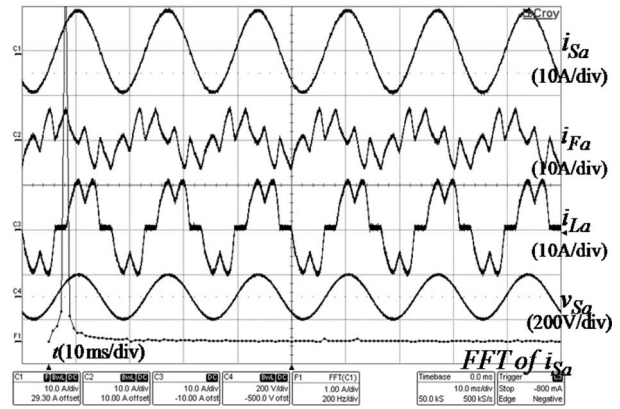
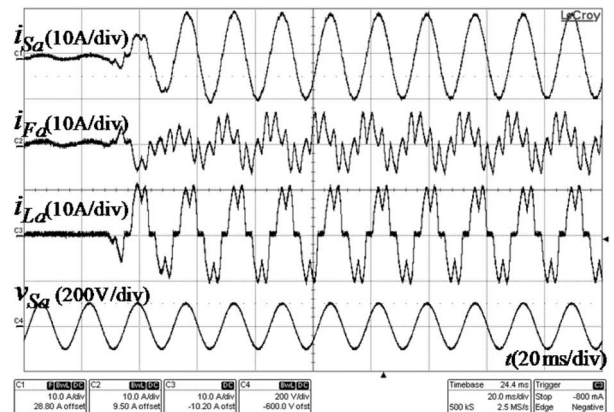
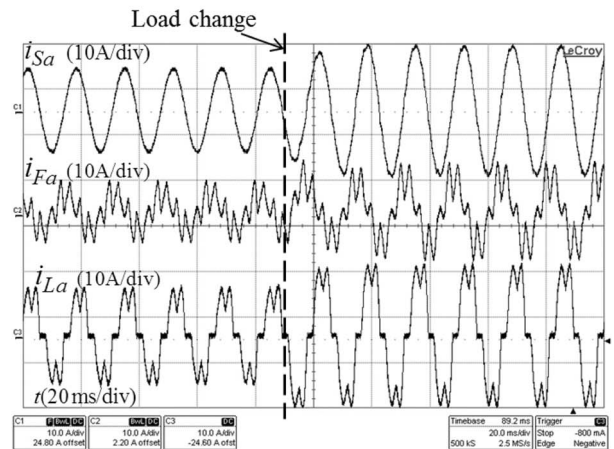


Fig. 15. Steady-state performance with proposed control scheme under RLC load.



(a)



(b)

Fig. 16. Dynamic responses of proposed control scheme under RLC load variations: (a) load applied (b) load changed.

condition is rare in practical networks. The non-sinusoidal supply voltage condition in practical networks may adversely affect the control performance of the APF. To verify the effectiveness of the proposed control algorithm under such conditions, experiments were carried out where the supply voltage was injected with fifth and seventh harmonic components of 10% and 5% magnitudes of the fundamental component, respectively. The results are illustrated in Fig. 17. As shown in Fig. 17, the harmonic compensation performance of the APF is not deteriorated by the distorted supply condition where the supply

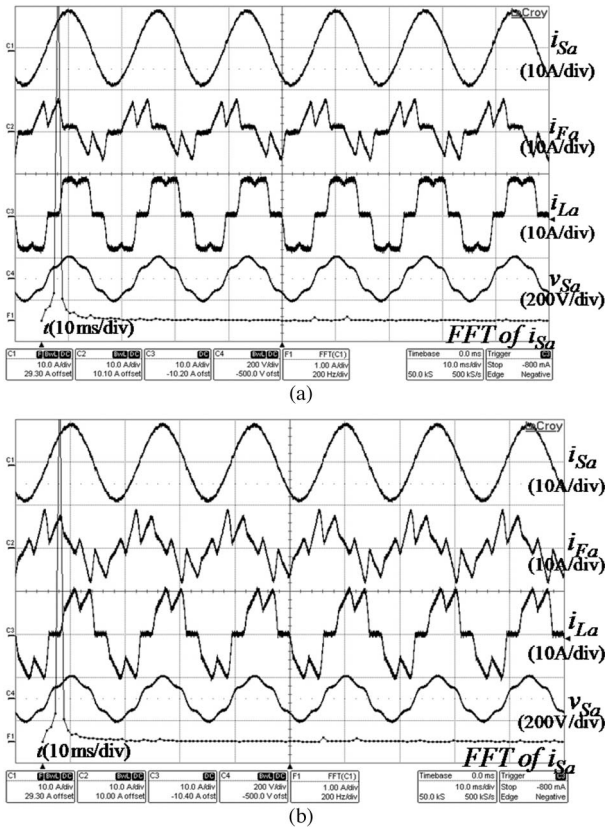


Fig. 17. Steady-state performance of the proposed control scheme under distorted supply voltage condition with (a) RL load and (b) RLC load.

current was also close to sinusoidal and similar with the results shown in Figs. 13 and 15 where an ideal sinusoidal supply voltage is given. There are only small increases in THD factors, approximately 1.84% and 1.93% for the cases of nonlinear RL and RLC loads, respectively.

The effectiveness of the proposed control strategy with the six-switch APF was validated through the results shown in Figs. 13–17. In addition, experimental tests with the four-switch APF are also carried out to completely verify the feasibility of the proposed control scheme with the four-switch APF where the steady-state performance under the nonlinear RL load and nonlinear RLC load are shown in Fig. 18(a) and (b), respectively. In Fig. 18(a), the capacitor voltages, V_{C1} and V_{C2} , were charged with the same value, i.e., 210 V, which is half of dc-link voltage, thus guaranteeing the balanced and robust operation of the proposed topology. There were very small variations in capacitor voltages, but it did not have a critical impact on the supply current performance, where the supply current was close to sinusoidal with a low THD factor of approximately 1.77%. Therefore, the experimental results verified that the four-switch APF is able to achieve good performance similar to that with the six-switch APF shown in Fig. 13 even though a fewer power switching devices is used. Similarly, the effectiveness of the four-switch APF was also confirmed under the nonlinear RLC load as shown in Fig. 18(b).

In addition, experimental tests for the four-switch APF under a distorted supply voltage condition are also carried out, and the obtained THD results are given in Table III. Table III shows a summary of the THD factors of the supply current achieved by

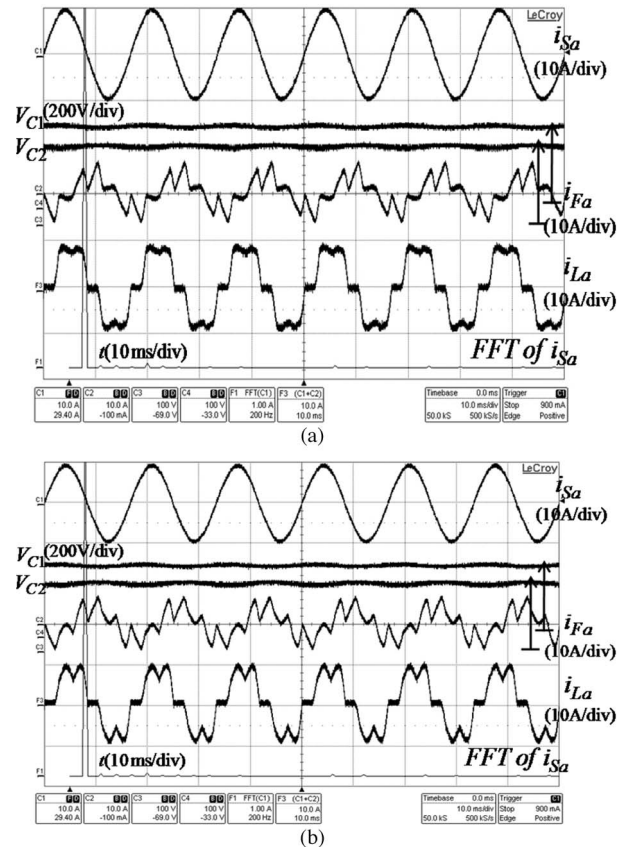


Fig. 18. Steady-state performances of the four-switch APF with (a) RL load and (b) RLC load.

the traditional PI current controller, and the proposed current controller under both ideal sinusoidal and distorted supply conditions, respectively. The results in Table III demonstrate that the proposed current controller achieves good performances under ideal sinusoidal as well as distorted supply conditions. The THD of the supply current is reduced to less than 2% for all cases. In contrast, such good performances cannot be achieved by using the traditional PI current controller. In the previous APFs, the THD values of the compensated supply current are normally around 2–5%, and the lowest THD up to now is about 1.2% in [18]. Even though the THD of the proposed current controller cannot reach the lowest value in [18], its THD is sufficiently small as compared with the results achieved in the other papers. Furthermore, the proposed APF is much cheaper since it uses only two current sensors and four switching devices. As a result, we can say the proposed APF has very good performance in spite of the reduced hardware, and it can be considered as a low-cost high-performance APF.

VI. CONCLUSION

In this paper, an advanced control strategy for the three-phase shunt APF was proposed. The effectiveness of the proposed control strategy was verified through various experimental tests, where the proposed control strategy presented good steady-state performance with nonlinear RL and RLC loads as well as good dynamic response against load variations: the supply current is almost perfect sinusoidal and in-phase with the supply voltage even under the distorted voltage condition. The experimental

TABLE III
COMPARISON OF THE THD FACTORS

Load	Load current THD	Traditional PI current controller	Proposed current controller			
			Six-switch APF		Four-switch APF	
			Ideal supply	Distorted supply	Ideal supply	Distorted supply
RL	24.4%	11.3%	1.65%	1.84%	1.77%	1.89%
RLC	30.2%	12.7%	1.72%	1.93%	1.86%	1.97%

results verified that the absence of a harmonic detector results in faster transient responses as well as assures notches free in steady-state performances of the supply current. Moreover, we also confirmed that the FSTPI can be used to implement the APF without any degradation in the APF performance. In all of the experiments, THD factor of the supply current was reduced to less than 2%, which completely comply with the IEEE-519 and IEC-61000-3-2 standards.

REFERENCES

- [1] *Recommended Practice for Harmonic Control in Electric Power Systems*, IEEE Std. 519-1992, 1992.
- [2] *Limits for Harmonic Current Emission*, IEC 61000-3-2, 2001.
- [3] H. Akagi, "New trends in active filters for power conditioning," *IEEE Trans. Ind. Appl.*, vol. 32, no. 2, pp. 1312–1332, Nov./Dec. 1996.
- [4] F. Z. Peng, "Application issues of active power filters," *IEEE Ind. Appl. Mag.*, vol. 4, no. 5, pp. 21–30, Sep./Oct. 1998.
- [5] H. Akagi, E. H. Watanabe, and M. Aredes, *Instantaneous Power Theory and Applications to Power Conditioning*, M. E. El-Hawari, Ed. New York: Wiley, 2007.
- [6] S. Buso, L. Malesani, and P. Mattavelli, "Comparison of current control techniques for active filters applications," *IEEE Trans. Ind. Electron.*, vol. 45, no. 5, pp. 722–729, Oct. 1998.
- [7] L. Malesani, P. Mattavelli, and S. Buso, "Robust dead-beat current control for PWM rectifiers and active filters," *IEEE Trans. Ind. Appl.*, vol. 35, no. 3, pp. 613–620, May/Jun. 1999.
- [8] S. Rahmani, N. Mendalek, and K. Al-Haddad, "Experimental design of a nonlinear control technique for three-phase shunt active power filter," *IEEE Trans. Ind. Electron.*, vol. 57, no. 10, pp. 3364–3375, Oct. 2010.
- [9] H. Hu, W. Shi, Y. Lu, and Y. Xing, "Design considerations for DSP-controlled 400 Hz shunt active power filter in an aircraft power system," *IEEE Trans. Ind. Electron.*, vol. 59, no. 9, pp. 3624–3634, Sep. 2012.
- [10] Z. Chen, Y. Luo, and M. Chen, "Control and performance of a cascaded shunt active power filter for aircraft electric power system," *IEEE Trans. Ind. Electron.*, vol. 59, no. 9, pp. 3614–3623, Sep. 2012.
- [11] L. Asiminoaei, F. Blaabjerg, and S. Hansen, "Detection is key—Harmonic detection methods for active power filter applications," *IEEE Ind. Appl. Mag.*, vol. 13, no. 4, pp. 22–33, Jul./Aug. 2007.
- [12] R. R. Pereira, C. H. da Silva, L. E. B. da Silva, G. Lambert-Torres, and J. O. P. Pinto, "New strategies for application of adaptive filters in active power filters," *IEEE Trans. Ind. Appl.*, vol. 47, no. 3, pp. 1136–1141, May/Jun. 2011.
- [13] Bhattacharya and C. Chakraborty, "A shunt active power filter with enhanced performance using ANN-based predictive and adaptive controllers," *IEEE Trans. Ind. Electron.*, vol. 58, no. 2, pp. 421–428, Feb. 2011.
- [14] F. A. S. Neves, H. E. P. de Souza, M. C. Cavalcanti, F. Bradaschia, and E. J. Bueno, "Digital filters for fast harmonic sequence component separation of unbalanced and distorted three-phase signals," *IEEE Trans. Ind. Electron.*, vol. 59, no. 10, pp. 3847–3859, Oct. 2012.
- [15] R. I. Bojoi, G. Griva, V. Bostan, M. Guerriero, F. Farina, and F. Profumo, "Current control strategy for power conditioners using sinusoidal signal integrators in synchronous reference frame," *IEEE Trans. Power Electron.*, vol. 20, no. 6, pp. 1402–1412, Nov. 2005.
- [16] C. Lascu, L. Asiminoaei, I. Boldea, and F. Blaabjerg, "Frequency response analysis of current controllers for selective harmonic compensation in active power filters," *IEEE Trans. Ind. Electron.*, vol. 56, no. 2, pp. 337–347, Feb. 2009.
- [17] L. Limongi, R. Bojoi, G. Griva, and A. Tenconi, "Digital current-control schemes," *IEEE Ind. Electron. Mag.*, vol. 3, no. 1, pp. 20–31, Mar. 2009.
- [18] C. Lascu, L. Asiminoaei, I. Boldea, and F. Blaabjerg, "High performance current controller for selective harmonic compensation in active power filters," *IEEE Trans. Power Electron.*, vol. 22, no. 5, pp. 1826–1835, Sep. 2007.
- [19] B. N. Singh, A. Chandra, and K. Al-Haddad, "Performance comparison of two current control techniques applied to an active filter," in *Proc. 8th ICHQP*, Athens, Greece, Oct. 14–16, 1998, vol. 1, pp. 133–138.
- [20] J. W. Dixon, J. M. Contardo, and L. A. Moran, "A fuzzy-controlled active front-end rectifier with current harmonic filtering characteristics and minimum sensing variables," *IEEE Trans. Power Electron.*, vol. 14, no. 4, pp. 724–729, Jul. 1999.
- [21] M. Singh, V. Khadkikar, and A. Chandra, "Grid synchronization with harmonics and reactive power compensation capability of a permanent magnet synchronous generator-based variable speed wind energy conversion system," *IET Power Electron.*, vol. 4, no. 1, pp. 122–130, Jan. 2011.
- [22] A. Szromba, "Energy controlled shunt active power filters," *Int. J. Comput. Math. Elect. Electron. Eng.*, vol. 26, no. 4, pp. 1142–1160, Jan. 2007.
- [23] E. Teresa and J. A. Pomilio, "Shunt active power filter synthesizing resistive load," *IEEE Trans. Power Electron.*, vol. 17, no. 2, pp. 273–278, Mar. 2002.
- [24] B. N. Singh, B. Singh, A. Chandra, P. Rastgoufard, and K. Al-Haddad, "An improved control algorithm for active filters," *IEEE Trans. Power Del.*, vol. 22, no. 2, pp. 1009–1020, Apr. 2007.
- [25] A. G. Yepes, F. D. Freijedo, J. Doval-Gandoy, O. Lopez, J. Malvar, and P. Fernandez-Comesana, "Effects of discretization methods on the performance of resonant controllers," *IEEE Trans. Power Electron.*, vol. 25, no. 7, pp. 1692–1712, Jul. 2010.
- [26] A. G. Yepes, F. D. Freijedo, O. Lopez, J. Malvar, and J. Doval-Gandoy, "High-performance digital resonant controllers implemented with two integrators," *IEEE Trans. Power Electron.*, vol. 26, no. 2, pp. 1692–1712, Feb. 2011.
- [27] F. Blaabjerg, D. Neacsu, and J. K. Pedersen, "Adaptive SVM to compensate DC-Link voltage ripple for four-switch three-phase," *IEEE Trans. Power Electron.*, vol. 14, no. 4, pp. 743–752, Jul. 1999.
- [28] M. B. de R. Corrêa, C. B. Jacobina, E. R. C. da Silva, and A. M. N. Lima, "A general PWM strategy for four-switch three phase inverter," *IEEE Trans. Power Electron.*, vol. 21, no. 6, pp. 1618–1627, Nov. 2006.



Quoc-Nam Trinh was born in Thanh-Hoa, Vietnam, in 1985. He received the B.S. degree in electrical engineering from the Ho Chi Minh City University of Technology, Ho Chi Minh City, Vietnam, in 2008. Currently, he is working toward the M.S./Ph.D. combined degree at the University of Ulsan, Ulsan, Korea.

His research interests are Z-source inverters, wind power systems, active power filters, and power quality.



Hong-Hee Lee (M'91–SM'11) received the B.S., M.S., and Ph.D. degrees in electrical engineering from Seoul National University, Seoul, Korea, in 1980, 1982, and 1990, respectively.

From 1994 to 1995, he was a Visiting Professor with Texas A&M University. Since 1985, he has been with the Department of Electrical Engineering, University of Ulsan, Ulsan, Korea, where he is currently a Professor in the School of Electrical Engineering. He is also the Director of the Network-based Automation Research Center, which is sponsored by the

Ministry of Knowledge Economy. His research interests are power electronics, network-based motor control, and control networks. Dr. Lee is a member of the Korean Institute of Power Electronics, the Korean Institute of Electrical Engineers, and the Institute of Control, Robotics, and Systems.